

A 94 GHz Spaceborne Cloud Profiling Radar Antenna System

Suzanne Spitz¹, Aluizio Prata, Jr.², Jefferson Harrell¹, Raul Perez¹, and Watt Veruttipong¹

Abstract --- The CloudSat spacecraft, scheduled to launch in 2003, will carry a 94 GHz cloud profiling radar. The electrical design of its antenna system has been completed and is presented here. It consists of a quasi-optical transmission line that performs signal relaying and duplexing, and a collimating antenna that provides the required gain and spatial resolution. An open Cassegrain geometry was selected because of its clear aperture, which allows for accurate electrical modeling, good performance, and significant reduction in implementation time and cost. The complete antenna system (horns to free space) has a worst case predicted gain of 63.1 dBi (59% efficiency) and exceeds the sidelobe envelope requirement of 50 dB below the peak gain at angles from boresight greater than 7 degrees.

Table of Contents

I.	INTRODUCTION
II.	SYSTEM DESCRIPTION AND REQUIREMENTS
III.	QUASI-OPTICAL TRANSMISSION LINE
IV.	COLLIMATING ANTENNA
V.	CONCLUSION
VI.	ACKNOWLEDGEMENT
VII.	BIBLIOGRAPHY

I. INTRODUCTION

The energy and water cycles present in the earth's atmosphere shape its climate characteristics. Since clouds are a basic part of the link between these two cycles, understanding their physical characteristics and associated seasonal and geographical variations is fundamental to meteorology. Climate prediction is currently limited by shortcomings on the understanding of where and how clouds form in the atmosphere. In recent years several radar instruments have been developed and operated to gather data on clouds, and hence overcome this problem.

The absorption present when looking through precipitation from the ground severely limits the radar sensitivity. It is therefore desirable to remotely sense the clouds from above. Two recently implemented instruments that approach these goals, and hence are particularly relevant to this work, are the Tropical Rainfall Measuring Mission Precipitation Radar (TRMM) [1] and the NASA DC-8 Airborne Cloud Radar

(ACR) [2]. The TRMM radar operates at 13.8 GHz and is the first spaceborne rain radar. It provides the three-dimensional structure of rainfall and hence some cloud data can be obtained from its measurements. The ACR is a 95 GHz airborne radar system developed specifically for remote sensing of clouds and their structure from an aircraft. A major objective of the ACR was to determine the feasibility of a future W-band spaceborne radar program. Its success paved the way for the CloudSat program and its 94 GHz nadir-pointing Cloud Profiling Radar (CPR), which is the subject of this work.

CloudSat will provide the first continuous global orbital survey of cloud structure and physical properties. The data gathered will improve the models used to describe clouds in global climate models. The CPR is expected to be several orders of magnitude more sensitive than available weather radars and hence will yield detailed observations of the water droplets and ice crystals in clouds. Unlike the ACR aircraft experiment, CloudSat's continuous data will allow the seasonal and geographical variations of clouds to be captured.

The key measurement provided by CloudSat is cloud reflectivity. Particles of water and ice are electrically small at millimeter wavelengths and their reflectivity is proportional to the fourth power of the radar operating frequency. It is therefore desirable to use a relatively high operating frequency. Aircraft experiments [2] have demonstrated that, with the appropriate radiated power, an instrument at 94 GHz is feasible and capable of yielding sufficient sensitivity to observe a wide range of clouds, spanning from the low stratocumulus type clouds to the high cirrus clouds.

The CloudSat spacecraft will be launched on a Delta II 7420-10 launch vehicle simultaneously with the NASA ESSP PICASSO-CENA (Pathfinders Instruments for Cloud and Aerosol Spaceborne Observations—Climatologie Etendue des Nuages et des Aerosols), a space-based aerosol and cloud lidar. Cloudsat will sit in the lower berth of the stacked fairing, under PICASSO-CENA. Once launched, the two spacecrafts (CloudSat and PICASSO-CENA) will fly in formation 705 Km above the earth surface, with CloudSat trailing one minute behind PICASSO-CENA. The two spacecrafts will complement each other, providing almost instantaneous lidar and radar views of the same segment of the atmosphere.

¹ Jet Propulsion Laboratory, California Institute of Technology, 4800 Oak Grove Dr, Pasadena, CA 91109-8099

² University of Southern California, Dept. of Electrical Engineering, Los Angeles, CA 90089-0271

In this work the preliminary electrical design and predicted performance of the CPR antenna system is presented.

II. SYSTEM DESCRIPTION AND REQUIREMENTS

The CloudSat radar consists of six primary subsystems as shown in the block diagram of Fig. 1. The digital subsystem performs the timing and control of the radar, and acquires and processes the reflectivity data. The upconverter generates and up-converts the lower frequency pulse to 94 GHz. The High Power Amplifier consists of an Extended Interaction Klystron (EIK), which amplifies the $3.33 \mu\text{s}$ long transmitted pulse to 1.5 KW peak, and a high voltage supply that provides 16 KV. The power distribution unit supplies power to all the low-voltage electronics.

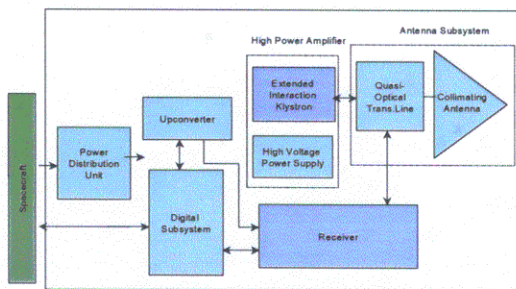


Figure 1: CloudSat Radar system block diagram

The antenna subsystem, which is shown in Fig. 2, consists of a quasi-optical transmission line (QOTL) and a collimating antenna. The QOTL couples the transmitted (or received) signal to (from) the collimating antenna and provides the required duplexing function to separate the transmitted and received 94 GHz radar pulses. The QOTL has three mirrors, a ferrite Faraday rotator, and a wire grid polarizer. The collimating antenna focuses the radiation and reception of the 94 GHz pulses with the required gain and radiation pattern. It has three mirrors: a large shaped primary (M1) that implements an ~ 1.85 meter diameter non circular radiating aperture, a shaped secondary (M2), and a third mirror (M3) that is used to relay the energy to the QOTL. Figure 3 shows a solid drawing of the antenna system at an early design stage. The M2 support structure is currently being designed and the projected M1 rim has been shaped.

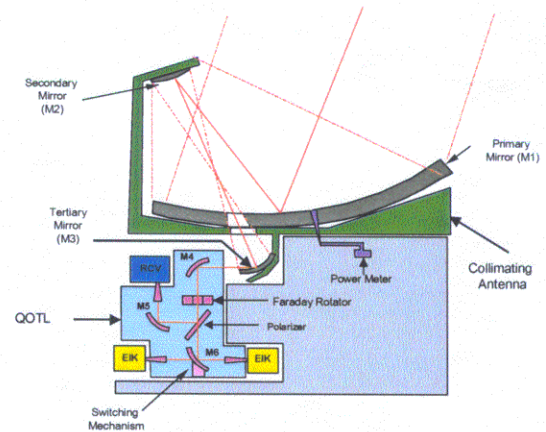


Figure 2: Antenna system block diagram

The CloudSat instrument is driven by several mission and science requirements. Particularly relevant to the antenna system is the 1.5 dB absolute reflectivity measurement accuracy requirement, the less than 2 Km diameter instantaneous radar footprint, the low sidelobe envelope (50 dB below gain peak for angles larger than 7 degrees from boresight), and the -26 dBZ minimum detectable cloud reflectivity at the end of the two years mission (dBZ is a weather radar unit that corresponds to dB relative to a reflectivity factor Z of $1 \text{ mm}^6/\text{m}^3$ [3]). These requirements drive the 94 GHz frequency choice, the collimating antenna topology and aperture size, and the required antenna system efficiency.

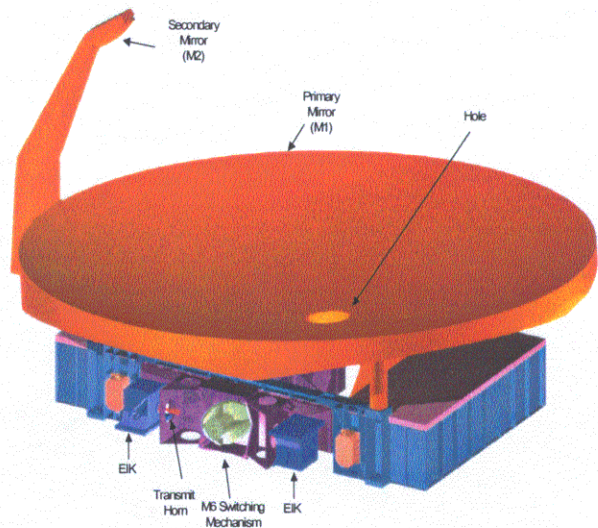


Figure 3: CloudSat antenna system

III. QUASI-OPTICAL TRANSMISSION LINE

The QOTL geometry depicted in Fig. 4., performs two functions in the CPR: signal relaying and duplexing. More specifically, when the CPR transmits the QOTL delivers the radio frequency energy pulse from the EIKs to the collimating antenna, and when the CPR receives the QOTL delivers the reflected signal from the collimating antenna to the receiver. Since the radiated transmitted and received signals have identical frequency and linear polarization, the required duplexing is accomplished through the use of a non-reciprocal component (a Faraday rotator) and a polarization grid located in the path common to both the transmitted and received signals [4]. The Faraday rotator creates a spatially orthogonal polarization relationship between the transmit and received signals, which are then separated by the polarization grid. Distinct feed horns are used to transmit and receive. To increase reliability, the CPR has two independent EIKs and associated feed horns, which are selected by the mirror M6 and its switching assembly. Note that all horns are identical, as well as mirrors M5 and M6.

The scale drawing of Fig. 4 details the QOTL and its operation. The transmitted 94 GHz pulse emanates from the active EIK in operation through its corresponding feed horn. The pulse then reflects at the switching mirror M6, passes through the polarizing grid, and then passes through the Faraday rotator, which spatially rotates the linear polarization by 45 degrees. From the Faraday rotator the beam reflects off the final QOTL mirror M4 and heads to the collimating antenna. The returned radar pulse is received by the collimating antenna and routed by M4 to the Faraday rotator, where the field is rotated an additional 45 degrees in the same direction as the transmitted pulse. The pulse leaving the Faraday rotator is then spatially filtered by the polarization grid, which reflects towards the mirror M6 (and receive horn) only the component orthogonally polarized to the transmitted signal at the polarization grid. Because of the net 90 degrees rotation, the pulse that reaches the receive horn is co-polarized with the transmitted pulse at the collimating antenna aperture.

The pulse relaying and duplexing tasks of the QOTL can in principle be accomplished by waveguides and circulators. However, the relatively large physical size of the EIKs determined their location on the CloudSat spacecraft bus and would have imposed relatively long waveguide runs. Since a typical WR-10 waveguide has about 3.3 dB/meter of loss at 94 GHz, the utilization of the QOTL (with its free-space propagation advantage) should yield substantially less loss to the antenna system.

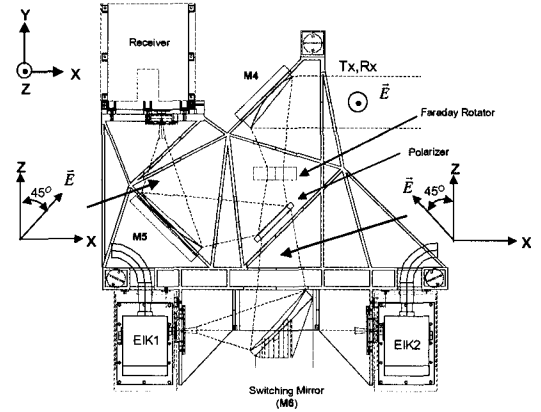


Figure 4: Quasi-Optical transmission line optical layout

To facilitate the QOTL and collimating antenna development efforts, a circular corrugated test horn was designed to provide test excitation to both mirror M4 of the QOTL and mirror M3 of the collimating antenna. With this horn the QOTL and collimating antenna can be developed and tested almost independently of each other, and combined only in the last stages of the program (an important convenience since the two systems are being completed separately). This is possible because, since the QOTL ultimately excites the collimating antenna, in the ideal case where the radiation pattern of M4 (with the QOTL transmitting) and the radiation pattern of M3 (with the collimating antenna receiving a plane wave) are conjugate matched, the coupling of the QOTL and the collimating antenna will have no loss due to pattern mismatch [5]. The design goal is then to have the QOTL and the collimating antenna match the pattern of the test horn, which was designed for practically invariant radiation pattern from the far zone up to at least 100 mm from the horn aperture. The radiation pattern of the test horn is depicted in Fig. 5.

Since one of the purposes of the QOTL is to relay energy, its mirrors have been designed for low spillover. The path from the EIK 1 to the collimating antenna has a total spillover of 0.16 dB, and the path from the EIK 2 (or receive horn) to the collimating antenna has a total spillover of 0.14 dB. The particular geometry adopted for the QOTL minimizes the number of mirrors at the expense of a somewhat worst collimating antenna coupling loss for the EIK 2 and receiver paths (0.45 dB), when compared to the EIK 1 path (0.25 dB). However, this degradation was deemed acceptable.

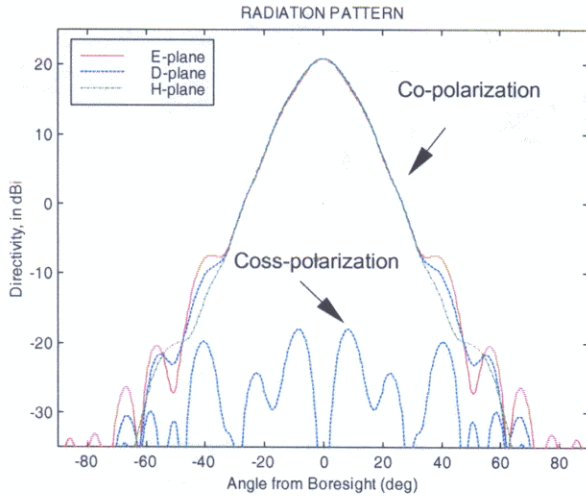


Figure 5: Test horn radiation pattern, measured on a 130 mm radius sphere centered on the phase center

IV. COLLIMATING ANTENNA

In the initial proposal for the CloudSat mission, an axially-symmetric Cassegrain collimating antenna was suggested. Due to blockage by the subreflector and its supporting structure, the axially-symmetric Cassegrain has inherently higher sidelobe levels and larger pattern prediction uncertainty than a clear aperture geometry. Since in a spaceborne atmospheric radar a large amount of earth surface clutter comes through the antenna sidelobes, the axially-symmetric Cassegrain geometry may yield intolerable sidelobe levels. To overcome this potential problem, CloudSat planned on implementing a frequency diversity scheme in its digital subsystem, where a slight frequency shift would be impressed in the sequence of transmitted pulses. This allows the cloud reflection to be separated from the surface clutter, alleviating the antenna sidelobe requirement. After the radar program was initiated, the use of an offset collimating antenna was proposed. The clear aperture of the offset geometry yields low sidelobes that can be accurately modeled. Due to this, the removal of the additional electronics needed to support the frequency diversity was also proposed and accepted.

The collimating antenna is severely constrained by the available spacecraft envelope (shown in Fig. 6) and several clear-aperture options were considered. Since there was no cross-polarization requirement, the highly compact open Cassegrain geometry was chosen [6]. This offset configuration, which is depicted in Figs. 3 and 6, offers excellent packaging characteristics and, although it requires a hole in reflector M1, it is free of all the other blockage scattering problems present in an axially-symmetric Cassegrain. The M1 hole increases the radiated sidelobe levels, but the hole can be made quite small and its scattering characteristics can be predicted with high degree of confidence. In fact, this high degree of confidence allows

the collimating antenna to be manufactured without the usual engineering and breadboard models, producing significant savings on both cost and implementation time.

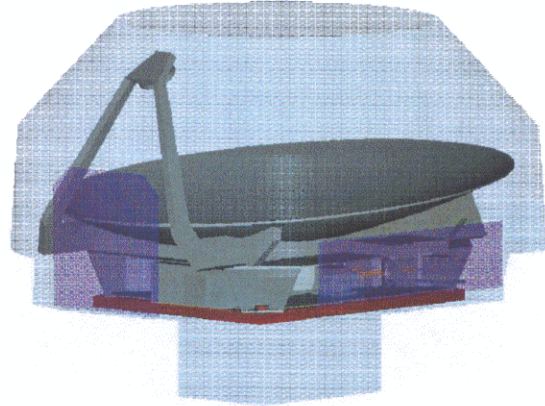


Figure 6: CloudSat instrument in spacecraft envelope

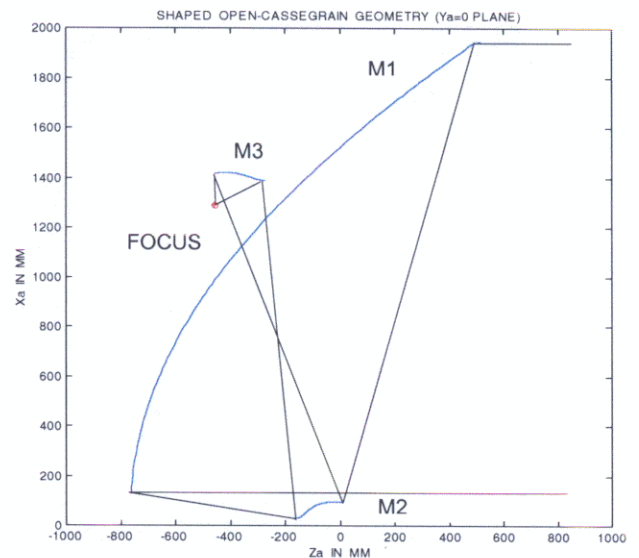


Figure 7: Scale drawing of the collimating antenna

Figure 7 depicts a scale drawing of the collimating antenna, which is discussed below in the transmit mode of operation. The mirror M3 surface is ellipsoidal and transforms the QOTL (or test horn) pattern from about 21 dBi gain to about 34 dBi gain at the surface of M2. The mirror M2 is shaped to provide an almost uniform amplitude illumination of the collimating antenna aperture. M1 is also shaped to correct the phase error introduced by the shaped M2. To maximize the gain, the rim of M1 is also shaped to optimize the utilization of the available spacecraft fairing envelope (the

projected M1 aperture is not circular). The end result is a projected collimating antenna aperture area of 2,798,018 mm², which yields a predicted 64.70 dBi directivity (85% efficiency since the maximum theoretical directivity of this aperture is 65.39 dBi), when excited by the test horn. This number does not include mechanical imperfections.

As mentioned previously, the radiation of M3 reaches M2 through a hole on the surface of M1. The hole is approximately elliptical in shape and has an aperture-projected major axis of about 110 mm. This assures small scattering by the hole and allows the collimating antenna to meet the sidelobe envelope requirement with more than 10 dB margin at 7 degrees from boresight.

The edge taper on M3 and M2 are 25 dB and 23 dB, respectively (space loss not included). On the hole the M3 radiation has a 30 dB edge taper. These high edge taper values yield a total spillover loss of only 0.16 dB for the entire collimating antenna (i.e., M3+hole+M2+M1).

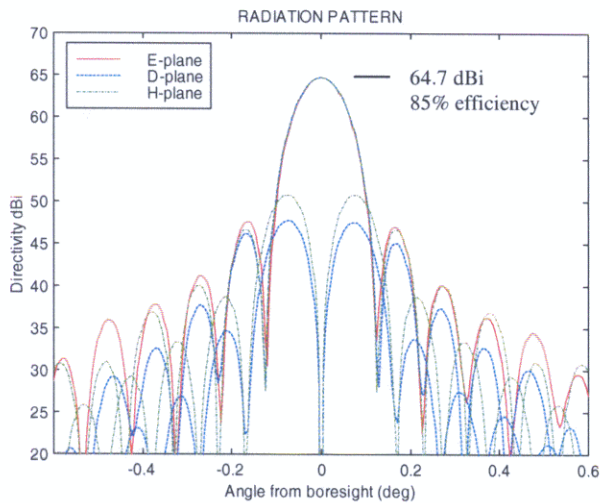


Figure 8: Collimating antenna near-boresight far-zone radiation pattern (excited by the test horn)

The near and far-from-boresight radiation patterns of the collimating antenna, when excited by the test horn, is depicted in Figs. 8 and 9, respectively. The near-boresight pattern was computed by sequentially using the physical optics (PO) technique starting from the test horn pattern and proceeding to M1 (the radiation of M3 through the M1 hole was modeled using the equivalence principle). Fig. 8 depicts the scattering of M1 and its hole, which are the only significant scattering effects in the angular range shown.

The far-from-boresight pattern of Fig. 9 is a composite result of two patterns that were computed using a combination of geometrical theory of diffraction (GTD) and PO scattering techniques [7]. This is needed because, for angles far from boresight, the required integration grid over M1 is very

dense and hence the computation time to determine the radiation pattern becomes prohibitively large. The first pattern of the composite was the radiation of M1 and its hole. It was obtained by first computing the radiation over M2, emanating from the M1 hole, as described for the near-boresight pattern. This pattern was then used to excite M2, and its scattering over M1 determined using GTD. The radiation from M1 and its hole was then determined using PO and plotted in Fig. 9. The second pattern of the composite is the M2 scattering and its spillover. It was determined as described for the near-boresight pattern and also plotted in Fig. 9. This composite pattern then shows, as an envelope, the dominant pattern of the two parts of the composite. Clearly seen in Fig. 9 is the effect of the M1 hole (oscillations that peak at about every 2 degrees, and can be seen between 2 and 30 degrees), and the M2 spillover (in the neighborhood of -70 degrees), the M1 top-rim spillover (beyond about -60 degrees). The -50 dB sidelobe envelope requirement (relative to peak gain) for angles greater than 7 degrees is met with ~12 dB of margin (worst case). Since the edge of the earth is at about 65° from nadir, the M1 and M2 spillovers do not contribute to clutter.

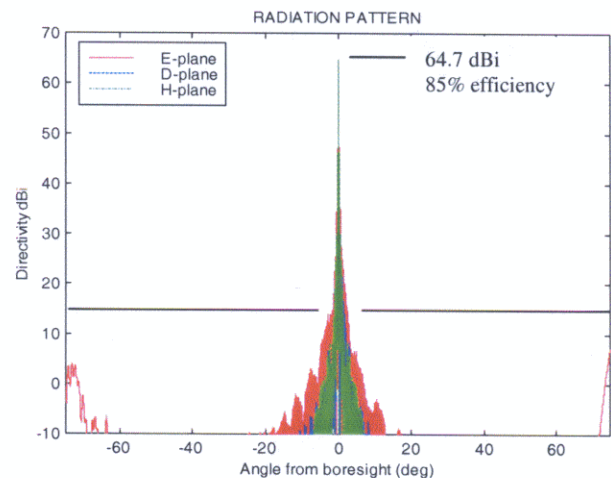


Figure 9: Collimating antenna far-from-boresight radiation pattern (excited by the test horn)

The mirror M1 and its associated support structure will be manufactured using composite materials to reduce weight while yielding an rms surface accuracy better than 25 μm. The surface of M1 will be coated with a vacuum-deposited aluminum film to provide a highly reflective surface at W-band. The mirror M2 will be machined in aluminum to an accuracy better than 25 μm. Both the M1 and M2 surfaces will subsequently be made Lambertian to reduce coherent scattering at infrared wavelengths, and hence minimize thermal loading. All other mirror surfaces (i.e., M3 – M6) will be machined of aluminum to an accuracy negligible compared to the surface accuracy of M1 and M2.

Table 1 summarizes the performance of the CPR antenna system, and provides a breakdown of its various loss components. As mentioned previously, the QOTL paths for the EIK 2 and the receiver have the worst performance with an overall gain of 63.1 dBi. The EIK 1 path has a better performance with a gain of 63.3 dBi. These numbers correspond to overall efficiencies for the CPR antenna system of 59.0% and 61.8%, respectively.

Loss/Gain Path Elements	EIK 1 (dB)	EIK 2 (dB)	RCVR (dB)
Collimating Antenna Directivity	64.70	64.70	64.70
Primary - Mirror M1			
Reflectivity	-0.04	-0.04	-0.04
Surface Error	-0.10	-0.10	-0.10
Secondary - Mirror M2			
Reflectivity	-0.012	-0.012	-0.012
Surface Error	-0.05	-0.05	-0.05
Tertiary - Mirror M3			
Reflectivity	-0.02	-0.02	-0.02
Surface Error	-0.012	-0.012	-0.012
QOTL to Collimating Antenna Coupling	-0.25	-0.45	-0.45
QOTL Mirror M4			
Spillover	-0.05	-0.05	-0.05
Reflectivity	-0.02	-0.02	-0.02
Surface Error	-0.012	-0.012	-0.012
Faraday Rotator			
Femite dielectric loss	-0.26	-0.26	-0.26
Matching Plates	-0.03	-0.03	-0.03
Reflectivity	0.00	0.00	0.00
Angular error	-0.03	-0.03	-0.03
Duplexing polarizer	-0.20	-0.20	-0.20
QOTL Mirror M5			
Spillover			-0.05
Reflectivity			-0.02
Surface Error			-0.012
QOTL Mirror M6			
Spillover	-0.05	-0.05	
Reflectivity	-0.02	-0.02	
Surface Error	-0.012	-0.012	
Feed Horn Waveguide Flange Pair	-0.10	-0.10	-0.10
Feed Horn & Waveguide Losses	-0.12	-0.12	-0.12
Total Overall Gain (dBi)	63.3	63.1	63.1

Table 1: Gain loss budget for the CPR antenna system

V. CONCLUSIONS

The electrical design of the CloudSat spacecraft cloud profiling radar antenna system has been completed. Currently the detailed mechanical design is in progress and manufacturing preparations are starting. The predicted results indicate that all required constraints have been satisfied. In particular, the antenna system has an overall gain larger than 63.1 dBi (59% efficiency), and a far-from-boresight sidelobe envelope that exceeds the required of 50 dB below the peak gain, at angles from boresight larger than 7 degrees. Since the final antenna is not yet available, only theoretical results have been presented here.

VI. ACKNOWLEDGEMENT

The research described in this paper was carried out by the Jet Propulsion Laboratory, under a contract with the National Aeronautics and Space Administration.

VI. BIBLIOGRAPHY

- [1] C. Kummerow, W. Barnes, T. Kozu, J. Shiue, and J. Simpson, "The Tropical Rainfall Measuring Mission (TRMM) Sensor Package," *J. Atmos. Oceanic Technol.*, Vol. 15, June 1998, pp. 809-817.
- [2] G. A. Sadowy, R. E. McIntosh, S. J. Dinardo, S. L. Durden, W. N. Edelstein, F. K. Li, A. B. Tanner, W. J. Wilson, T. L. Schneider, and G. L. Stephens, "The NASA DC-8 Airborne Cloud Radar: Design and Preliminary Results," *Proc. of the International Geoscience and Remote Sensing Symposium (IGARSS)*, Singapore, Aug. 3-8, 1997.
- [3] R. Meneghini and T. Kozu, *Spaceborne Weather Radar*, Chap. 2, Artech House, Inc., 1990.
- [4] G. M. Smith, C. P. Unsworth, M. R. Webb, and J. S. G. Lesurf, "Design, Analysis and Application of High Performance Permanently Magnetized, Quasi-Optical, Faraday Rotators," 1994 IEEE MTT Symposium Digest, pp. 293-296.
- [5] M. K. Hu, "Near-Zone Power Transmission Formulas," 1958 IRE National Convention Record, New York, N. Y., March 24-27, 1958, Part 8, pp. 128-138.
- [6] W. V. T. Rusch, T. S. Chu, A. R. Dion, P. A. Jensen, and A. W. Rudge, "Quasi-Optical Antenna Design and Applications," on *The Handbook of Antenna Design*, edited by A. W. Rudge, K. Milne, A. D. Olver, and P. Knight, Peter Peregrinus Ltd., 1982, Chap. 3.
- [7] W. V. T. Rusch and P. D. Potter, *Analysis of Reflector Antennas*, Academic Press, 1970.